



# Monitoring and Numerical Analyses of the Steel Railway Arch Bridge: A Case Study

Piotr Olaszek, Ph.D.<sup>1</sup>; Andrzej Świercz, Ph.D.<sup>2</sup>; Ireneusz Wyczałek, Ph.D.<sup>3</sup>; and Przemysław Kołakowski, Ph.D.<sup>4</sup>

**Abstract:** The subject of research is a steel arch-tied bridge at a high-speed railway line in Poland. After the construction was completed, a resonance phenomenon was observed at the bridge, consisting of the occurrence of intense (visible to the unaided eye) undamped vibrations of some vertical hangers in the horizontal direction, transverse to the track axis. These vibrations occurred without the presence of a railway load on the bridge. Before the bridge was put into operation, an acceptance static and dynamic load test was performed, and then the bridge deck vibrations were monitored for a year. The research during dynamic loads testing included both quasi-static (10 km/h) and high-speed (200 km/h) testing train passages. The vertical displacement measurements were carried out in three cross sections of the span, and the acceleration of vibrations on girders and selected hangers was also measured. Next, an innovative system for determining displacements indirectly using inertial sensors (inclinometers and accelerometers) was used for bridge deck vibration monitoring. The primary aim of the research was to investigate the possibility of assessing the safe operation of the bridge using a monitoring system consisting of a limited number of inertial sensors. The second aim was to verify the feasibility of calibrating the numerical model based on the results of dynamic load testing. Numerical analyses of the behavior of the bridge during the passage of trains with speeds up to 200 km/h were carried out. The developed and calibrated numerical model provides additional information about the overall structural vibrations, facilitating the interpretation of outcomes of the monitoring system. No significant impact of hanger vibrations on the monitored displacements and accelerations of the bridge deck vibrations during the passage of trains was found. DOI: 10.1061/JBENF2.BEENG-6962. This work is made available under the terms of the Creative Commons Attribution 4.0 International license, <https://creativecommons.org/licenses/by/4.0/>.

**Author keywords:** Arch-tied railway bridge; Bridge monitoring; Load testing; Bridge vibration; Numerical model calibration.

## Introduction

Railway steel arch bridges, due to their specific dynamic properties, are often the subject of scientific and research work. The research conducted is most often related to numerical analyses supported by short-term field testing of structures or long-term monitoring. Lacarbonara and Colone (2007) investigated the dynamics of simplified planar arch bridges using analytical and semianalytical approaches. Ribeiro et al. (2012) presented a three-dimensional (3D) numerical model that is tuned using modal parameters obtained by testing an arch bridge. The calibration process was based on a genetic algorithm, followed by a numerical model validation based on experimental, dynamic tests under railway traffic. The resonant effects of traveling trains over arch bridges were analyzed by Ju and Lin (2003). A 3D beam-shell model presented by

Zeng et al. (2018) was used for the analysis of the vehicle-steel arch bridge interaction where the trains are considered multibody assemblies. The proposed method employed three solvers: vehicle, bridge, and interaction. A numerical model of the six-span structure carrying railway tracks was prepared. The mass of the concrete ballast was accounted for in computations; however, its stiffness was not considered. Zhao et al. (2019) identified the temperature-induced/train-induced deflections of the same bridge girder from deflection data obtained from the wavelet transform. Ding et al. (2017) drew attention to the effects of train-induced transverse vibration on the train running stability at the same bridge. Calçada et al. (2002) described experimental and numerical dynamic analyses of an old arch double-deck iron bridge when subjected to the moving loads of the new light metro. Results obtained from numerical simulations conducted on the basis of an experimentally calibrated finite-element model, both in terms of structural safety and comfort of pedestrians and train passengers, are presented.

Hangers are a specific element of the arch bridge structure. Malm and Andersson (2006) presented large vibrations of the hangers of a steel arch-tied railway bridge, which were observed during train passages. The low damping in the hangers has a large influence on the risk of fatigue failure. Andersson et al. (2015) studied the use of passive and adaptive damping systems to mitigate vibrations in the same bridge during resonance. Duan et al. (2022) conducted train-induced dynamic response and fatigue damage analyses for the hangers of an arch-tied railway bridge. Ding et al. (2016) presented field monitoring of the train-induced hanger vibration in the previously presented bridge and stated that there is no correlation between vibration amplitudes of the hanger and the main girder. Zhong et al. (2018) analyzed the fatigue behavior evaluation of hangers at this bridge. Salamak et al.

<sup>1</sup>Associate Professor, Road and Bridge Research Institute, ul. Instytutowa 1, 03-302 Warszawa, Poland (corresponding author). ORCID: <https://orcid.org/0000-0003-0219-4219>. Email: polaszek@ibdim.edu.pl

<sup>2</sup>Main Specialist, Institute of Fundamental Technological Research, Polish Academy of Sciences, Adolfa Pawińskiego 5B, 02-106 Warszawa, Poland. Email: aswiercz@ippt.pan.pl

<sup>3</sup>Associate Professor, Institute of Civil and Environmental Engineering and Architecture, Bydgoszcz Univ. of Science and Technology, Al. prof. S. Kaliskiego 7, 85-796 Bydgoszcz, Poland. ORCID: <https://orcid.org/0000-0003-3963-8186>. Email: ireneusz.wyczalok@pbs.edu.pl

<sup>4</sup>Chief Executive, Adaptronica Sp. z o.o., ul. Szpitalna 32, 05-092 Lomianki, Poland. Email: przemyslaw.kolakowski@adaptronica.pl

Note. This manuscript was submitted on April 2, 2024; approved on September 10, 2024; published online on October 22, 2024. Discussion period open until March 22, 2025; separate discussions must be submitted for individual papers. This paper is part of the *Journal of Bridge Engineering*, © ASCE, ISSN 1084-0702.

(2023) presented the finite-element model updation of steel hangers in an existing railway steel arch bridge based on vibration signals acquired from the long-term vibration-based structural health monitoring system.

This paper presents a case study of field tests and numerical analyses of a steel arch bridge at a high-speed railway line in Poland. Before putting the bridge with a single railway line into service, static and dynamic load tests were carried out. Before conducting the static tests, the presence of intense (visible to the unaided eye) undamped vibrations of some hangers in the horizontal direction transverse to the track axis had been noticed. These vibrations occurred without the presence of a railway load on the bridge. During the 3 weeks before the dynamic test, this phenomenon occurred irregularly. There were days without the occurrence of such vibrations visible to the unaided eye. A similar resonance phenomenon appearing at a steel railway bridge, which was visible on the slender hangers connecting the arch girder and the main truss girder under certain wind conditions, was presented by Link et al. (2002).

The measurements under static and dynamic loads and numerical analyses did not indicate a decrease in the load capacity of the structure due to the hanger vibrations. The bridge was put into service, and vibration monitoring of the hangers was performed. A similar phenomenon, but with smaller vibration amplitudes, also occurred on the twin span (separate structure) serving the opposite direction of the railway. For a year, the bridge deck vibrations were monitored both with and without the load of moving trains under the influence of wind, temperature changes, and insolation. In the first 2 months of monitoring the behavior of the bridge deck, the hangers were not modified. In the remaining period, masses concentrated in the middle of the length of the hangers were added to the hangers, modifying the frequencies of their vibrations. Eventually, this solution was abandoned, and the hangers were replaced with new ones that allowed for adjusting the tension force. This was done after the end of the presented monitoring of the bridge deck behavior. Further studies and analyses related to the hanger vibrations and their potential fatigue were carried out by other teams and are the subject of a separate publication (Bleja and Żółtowski 2021).

The field tests used for the calibration of the numerical model, as well as the first 2 months of the monitoring period, were conducted without the masses installed on the hangers for vibration reduction. Both ends of the hangers were welded, preventing any adjustment of the tension forces. The numerical model did not include the concentrated masses that were later installed after the numerical model calibration was completed. Numerical analyses showed no impact of the tension force on the displacement and acceleration deck due to moving loads. The beating vibrations also occurred after the installation of the concentrated masses but with a slightly smaller amplitude. The beating effect occurred both during train passages and when no train was on the bridge.

Due to the use of an innovative system for monitoring displacements and accelerations, the research presented in the paper is of a cognitive and practical nature. The basic cognitive objective of the presented research was to verify the possibility of bridge deck vibration and deflection monitoring using a measurement system consisting of a limited number of inertial sensors.

The basic practical objectives of the presented research included

1. verification of the feasibility of calibrating the numerical model based on the results of the dynamic load testing and its use during the service of the bridge; and
2. monitoring bridge deck vibrations in the presence of poorly damped vibrations of hangers.

## Railway Arch Bridge

### Description of the Structure and Its Numerical Model

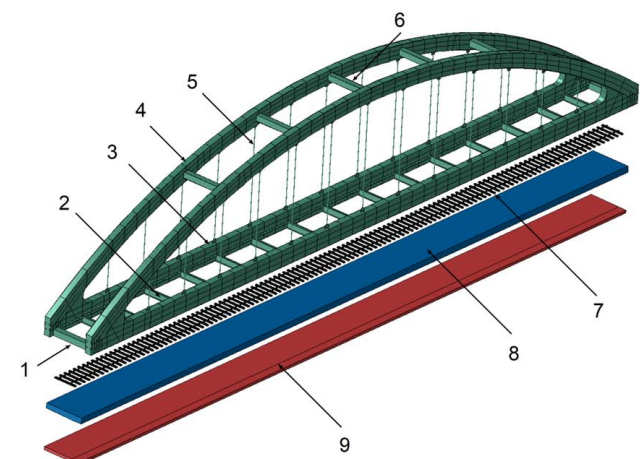
The bridge consists of two separate steel arch structures, each for a single rail track. The span of both bridge structures is 75.00 m (Fig. 1). Each of the structures was designed for train speeds up to 250 km/h, and after load testing, it was approved for this speed, with the condition that additional experimental verification would be required for train speeding above 200 km/h. However, during the initial monitoring period, the maximum speed was 160 km/h, which was later increased to 200 km/h after 5 months. A general view of the components included in the numerical model for a single structure is illustrated in Fig. 1(c). The main



(a)



(b)



(c)

**Fig. 1.** Tested bridge: (a) side view; (b) view from the track level; and (c) modeled structural components of the bridge: 1 = box section cross beam; 2 = I section cross beam; 3 = beam girder; 4 = arch girder; 5 = hanger; 6 = lateral bracing; 7 = track; 8 = ballast; and 9 = concrete slab. (Image by Piotr Olaszek.)

steel structure consists of a pair of parallel arch girders, rigidly connected using five lateral bracings and a pair of horizontal beam girders linked to each other by means of 17 cross beams. The arch and beam girders are connected using 13 evenly distributed pairs of hangers modeled by the Euler–Bernoulli beam elements. The hangers were welded to the arch and beam girders without possibly adjusting the tension force. For the numerical model purposes, the hangers' tension force values were taken from the technical documentation of the bridge. At support zones, the arch and beam girders were joined together.

Due to their complex closed box cross sections, all girders, side braces, and the two extreme transverse beams were modeled using shell elements. The model includes longitudinal and transversal internal stiffeners of the girders. The shell elements were also applied for the remaining 15 equidistant cross I-beams linking beam girders. A concrete slab was installed on the upper side of the cross beams using steel bolts. The concrete slab, analogous to the railway ballast, was modeled by hexahedral elements. The kinematic constraints couple the generalized displacements between the cross beams and the concrete slab and between the concrete slab and railway ballast.

The railway ballast directly supports the railway track, which consists of 121 concrete sleepers and 2 rails. The track was modeled by Euler–Bernoulli beams.

Both the concrete plate (approximately 35 cm thick) and the railway ballast (approximately 62 cm thick, with Young's modulus of 0.15 GPa and a density of 1,100 kg/m<sup>3</sup>) were modeled as separate, homogenized elastic layers using brick elements. In contrast, the railway track was implemented using Bernoulli beam elements: sleepers (16 × 23 cm) were modeled with a rectangular cross section, and rails (type UIC 60) were modeled with a generalized cross section.

The model and analyses were performed using Abaqus (version 6.24) (2024) software. For the first computation purposes, the material data were taken from the technical documentation of the bridge. Subsequently, Young's modulus of the concrete slab, the density of the railway ballast, and the damping parameters were updated in a two-stage process of numerical model calibration, which is discussed in the section "Numerical Model Calibration."

### Scope of Measurements during Load Testing and Monitoring during Operation

During the static and dynamic load testing, measurements of vertical displacements were taken at three cross sections of the span, located at 1/4, 1/2, and 3/4 of the span. During load testing, the highway traffic under the bridge was partly limited, which allowed the application of inductive gauges located under the bridge. Wires were attached at one end to the girder at the measurement location points and at the other end to springs fixed to the ground. Sensors (inductive gauges) were attached to the wires. During the dynamic tests, the acceleration of vibrations on girders and selected hangers was also measured. An innovative system for determining displacements indirectly using inertial sensors (inclinometers and accelerometers) was used for monitoring. Inclinometers were installed in one line on a bridge span, and an accelerometer was installed at the point of displacement examination. Signals from inclinometers were used to determine the so-called quasi-static component of the displacement, while signals from the accelerometer were used to determine the dynamic component. Details of the sensors and algorithms used for signal processing and indirect displacement determination are presented in Olaszek et al. (2020). For testing purposes, a limited number of sensors were applied. Extreme displacement values were determined and compared with numerically determined values, whereas extreme amplitudes of vibration

acceleration in specific frequency ranges were compared with permissible or numerically determined values. A diagram of the location of measurement points is presented in Fig. 2.

## Bridge Load Testing and Numerical Model Calibration

### Specific Behavior of the Hangers

Before the static tests of the first span began, the presence of intense (visible to the unaided eye) undamped vibrations of some hangers in the horizontal direction transverse to the track axis was noticed. The accelerations of the vibrations of one of the hangers (No. 8HR), recorded at 1/4 length, are presented in Fig. 3.

The double vibration amplitude of the hangers was determined by double integration of the recorded acceleration fragment. The double integration error was reduced by removing any linear trends to obtain symmetric vibrations about the zero position. The determined displacement history was also verified by the double integral of the trigonometric function with known frequency and amplitude. The obtained value of the double amplitude of displacement was approximately 4 mm at 1/4 of the length of the hanger, which, due to the shape of the modal vibrations, indicates that a double amplitude of displacement (at 1/2 of the hanger length) was about 8 mm. There were two similar frequencies in the spectrum of measured vibration accelerations (5.078 and 5.099 Hz). A very small difference in the natural frequencies of only about 0.02 Hz was the reason for the beating phenomenon, i.e., the overlapping of vibrations leading to oscillations with very large amplitudes. Beating is an internal resonance in which slight external excitations, such as vibrations caused by the road traffic under the bridge or gusts of wind, can cause very large amplitudes of vibrations. It was also observed that high-amplitude vibrations were transmitted from one hanger to another, both within one arch and to the adjacent arch, and there was significant excitation of vibrations of hangers during the passage of trains.

The hangers are bars made of Y1880 steel with Young's modulus of 195 GPa and a circular cross section with a diameter of 80 mm. The considered hanger (No. 8) has a length of 11.003 m and a designed tension force of 255.4 kN. This yields a uniform stress level of 50.8 MPa in the bar and a computed first natural frequency of 4.97 Hz. The relationship between the calculated natural frequency of the hanger (No. 8) and the tension force, expressed by uniaxial stress level, was determined. The estimated stress level for the measured dominant natural frequency of 5.099 Hz was equal to 55.15 MPa, which implies a slightly higher tension force (277.2 kN) than the designed one, an increase of 8.5%.

On both sides of the bridge, the ends of each hanger were welded to the horizontal girder and the arch. As a consequence of the characteristics of welded joints, fatigue failures appear in welded structures mostly at the welds rather than in the base metal, even if the latter contains notches such as openings or re-entrant corners (Fricke 2003). An example of a threat is the study of a railway bridge by Klinger et al. (2014), which shows a fatigue crack near a butt weld of a hanger. Moreover, the evaluation of welded joints is complicated, especially with fillet welds that are more sensitive to fatigue stresses. Also, it is recommended to carry out additional ultrasonic tests (Berthelley 2018).

Due to the adverse nature of the problem in the case of the railway arch bridge presented here, the attenuation of ambient-induced hanger vibrations was also handled by a separate team (Bleja and Żótkowski 2021). Negative dynamic behavior of the hangers in a tie arch bridge may result locally from insufficient tension under dead load. Such a situation may occur because of objective assembly imperfections. The results of measurements under static and

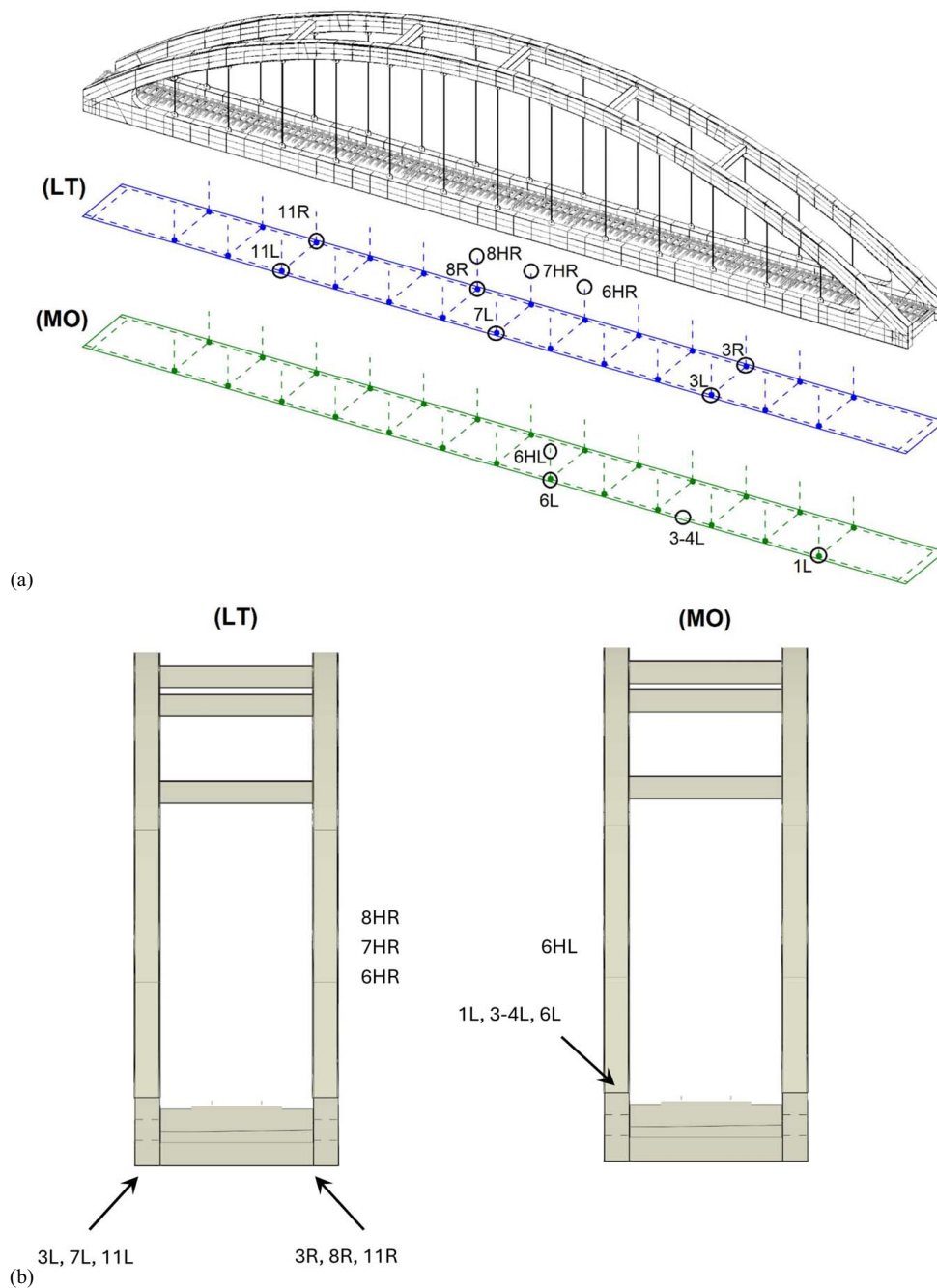


**Fig. 2.** Diagram of measuring points' location in (a) isometric; and (b) cross-sectional views. LT = load testing; 3L, 3R, 7L, 8R, 11L, and 11R = points of deck vertical displacement measurement and deck vibration acceleration measurement; 6HR, 7HR, and 8HR = points of hanger vibration acceleration measurement; MO = monitoring; 1L, 3-4L, and 6L = points of deck inclination measurement; 3-4L = point of deck vibration acceleration measurement and deck vertical displacement monitoring; 6HL = point of hanger vibration acceleration measurement. The numbering of points is consistent with the numbering of hangers; L and R stand for the left and right sides of the viaduct, respectively.

dynamic loads and numerical analyses did not indicate a decrease in the load capacity of the structure due to the hangers' behavior described previously. Based on the numerical model of the isolated hanger (No. 6) and the assessment of the amplitude of beating vibration of the hanger (approximately 4 mm at 1/4 of the length of the hanger), the resulting stress from vibration and tension (von Mises—Rao 2017) at its ends was evaluated at the level of 60 MPa. This value is much lower than the ultimate strength of the hangers (1,880 MPa) and connectors ( $\geq 490$  MPa). However, due to the risk of fatigue, remedial work was undertaken to reduce vibrations. In the first stage, mass weights were installed on the

hangers to change the inertia of the system. However, the ambient-induced vibration levels were still present with only a reduction in amplitude. For this reason, the railway authorities soon decided to replace the hangers with ones having adjustable tension. After replacing the hangers, the vibrations generated by environmental factors were eliminated.

### Numerical Model Calibration

The bridge is a relatively new structure, and its numerical model was developed based on the design documentation. The numerical

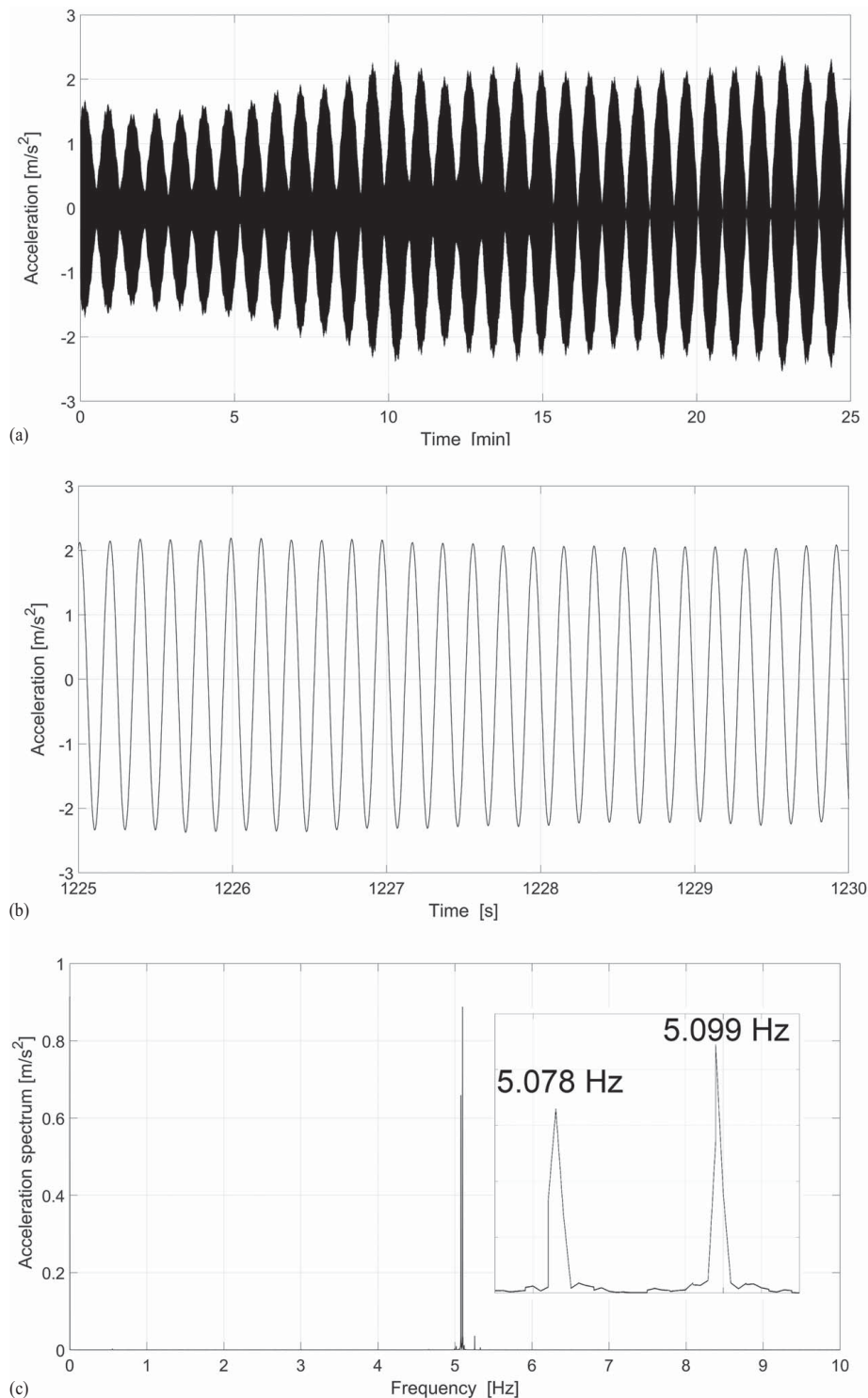


**Fig. 3.** Accelerations of vibrations of one of the hangers (No. 8HR) recorded at 1/4 length before starting the static tests (with 10-Hz low-pass filtering): (a) nonstopping vibrations recorded for over 25 min; (b) 5-s fragment of vibrations from about 20 min of recording; and (c) spectral analysis of vibrations with additional fragment magnification of about 5.090 Hz.

model was calibrated using the results of tests conducted during load testing of the bridge. Load testing involved the operation of a test train, comprising two ES64U4 locomotives and four passenger cars of Type 154A, traveling at speeds of 10 km/h (quasi-static speed) and 200 km/h (maximum allowed speed).

The recorded displacement and acceleration profiles were used for the calibration of the numerical model of the structure. Model calibration was carried out in two stages.

1. Calibration with quasi-static load testing at a train speed of 10 km/h, aimed at determining the Young's modulus of the concrete slab.
2. Calibration with dynamic load testing at a train speed of 200 km/h, aimed at determining Rayleigh damping parameters and the modeled mass of the viaduct—in this case, it was adjusted by altering the density of the railway ballast preserving its design volume.

**Table 1.** Parameters for the calibration and discretization of the numerical model and the estimated values

Parameter	Range	Step	Estimated value	Calibration type
Young's modulus (concrete) (GPa)	32–36	1	35	Static
Density (railway ballast) (kg/m <sup>3</sup> )	700–1,500	200	1,100	Dynamic
Rayleigh damping parameter $\alpha$	0.2–0.5	0.05	0.35	Dynamic
Rayleigh damping parameter $\beta$	0.002–0.005	0.0005	0.004	Dynamic

The calibration of the numerical model was performed by comparing the measured displacements with computed displacements at the 1/4, 1/2, and 3/4 span lengths (Locations 3L, 7L, 8R, 11L, Fig. 2) for a predetermined range of the parameter under investigation. In the first stage of calibration, all cross sections were taken into account, and in the subsequent ones, due to relatively small displacement values, the central cross section was omitted. For each parameter value (i.e., concrete slab Young's modulus for quasi-static load testing) and set of parameter values (i.e., railway ballast density and Rayleigh damping parameters for dynamic load testing), the structural responses were recalculated. The value of the parameter for which the smallest sum of absolute differences between the computed and measured displacements was obtained was considered established and used for further calculations. For the calibration with quasi-static loading, a passage of the test train at a speed of 10 km/h was used, where the stiffness of the structure predominantly affects the deflection. As a result of the numerical calculations, Young's modulus value of 35 GPa for the concrete slab was obtained. The ranges of the considered parameters for the numerical model calibration, their discretization, and the estimated values are summarized in Table 1.

The results and comparison of the numerical modal analysis and the spectral analysis of the measured displacements and accelerations regarding the free vibrations are presented in Table 2. The conformity of the calculated and measured two lowest eigen frequencies for lateral vibrations was 104% and for vertical vibrations 103%. In the case of modal shapes corresponding to higher natural frequencies, these discrepancies are slightly larger, ranging from 91% to 111%.

The damping of free vibrations was defined by determining the logarithmic damping decrement (LDD) on the basis of the displacement waveforms. Due to the presence of one dominant vibration frequency, it was possible to determine it directly without using band-pass filtering or other methods to utilize knowledge of amplitude beat presence (Nakutis and Kaškonas 2011). The LDD determined on the basis of measurements was in the range of 0.1798–0.2050 (equivalent to the damping ratio  $\xi$  within the range of

0.0286–0.0326), while in the numerical model, it was assumed as  $\xi = 0.0369$ . This corresponds to the compliance of the numerical model with the measurement results within the range of 113%–129%.

The presented analysis also focused on the selection of a moving load model. The load from a passing train was modeled using two approaches: the moving concentrated forces model (MCFM), which assumes the same axle load in a specific section of the rail vehicle, evenly distributed over two rails, and the moving inertial mass model (MIMM), which considers the interaction between the rail and the vehicle (mass element sliding on the rail), accounting for inertial effects on structural vibrations. In the case of calibration with dynamic load testing, a passage of a test train at a speed of 200 km/h was used.

In the MCFM approach, each axle load is modeled using a pair of concentrated forces, with one force acting on each rail and proportionally distributed among the adjacent rail nodes. In contrast, the MIMM method utilizes contact phenomena to describe the load transfer to the rails. Both of these load scenarios, depending on the train speed, have been implemented as batch files.

For both the MCFM and MIMM models, a railway ballast density of 1,100 kg/m<sup>3</sup> was obtained (assuming a constant design volume of railway ballast). Following the described procedure, the Rayleigh damping parameters were determined ( $\alpha = 0.35$ ,  $\beta = 0.004$ ).

The comparison of measured and calculated (with the use of MCFM and MIMM) vertical displacement of the beam girder near Hanger no. 3 (extreme displacement section) during a test train passage with a speed of about 200 km/h is presented in Fig. 4(a). Analogous comparison of measured and calculated vertical acceleration of beam girder vibration near Hanger no. 8 (section of high-level hanger vibrations) during a test train passage with a speed of about 200 km/h is presented in Fig. 4(b). The low-pass filter of 30 Hz was applied to all the calculated and measured time histories of acceleration. In the case of bridge deck vibrations, the 30 Hz filtration limit frequency results from the ballast stability conditions (Calgaro et al. 2010). Fig. 4(c) shows the acceleration

**Table 2.** Results and comparison of the theoretical modal analysis and spectral analysis of the measured displacements and accelerations of free vibrations

Mode no.	Calculated		Measured			Conformity Calculated/measured (%)
	Characteristics of mode shape	Modal frequency (Hz)	Bridge element	Direction	Frequency (Hz)	
1st	Symmetric lateral bending of the arch (D) and torsion of the deck	0.94	Arch	Lateral	0.90	104
			Deck	Lateral	0.92	102
2nd	Antisymmetric vertical bending of the full bridge	1.87	Deck	Vertical	1.82	103
3rd	Antisymmetric torsion of the full bridge	2.17	Deck	Vertical	1.95	111
			Arch	Lateral	2.16	100
4th	Antisymmetric vertical bending of the full bridge	2.60	Deck	Vertical	2.86	91
—	—	—	—	—	—	—
17th	Symmetric vertical bending of the full bridge	3.24	Deck	Vertical	3.03	107
—	—	—	—	—	—	—
35th	Symmetric vertical bending of the full bridge	5.26	—	—	—	—

Notes: The terms antisymmetric or symmetric refer to the direction along the bridge. Dominant vibrations are marked (D). Selected mode shapes are presented; hanger vibrations (local modes) dominate in Modes 5–16 and 18–34.

frequency spectra of the measured and calculated bridge deck vibration. In the signals recorded by measurement sensors, two frequencies (3.0 and 6.2 Hz) dominate, while the frequency contributions in numerically modeled responses are mainly dispersed across lower frequencies; also, bridge vibrations modeled under inertial loading are observed in the frequency range above 6.2 Hz.

The comparison of the calculated displacements of forced vibrations with the measured one was carried out using two parameters. The first parameter, which is commonly used, is the mean absolute percentage deviation (MAPD) of the peak values (negative or positive) of the calculated and measured displacements as determined by the following equation:

$$\text{MAPD} = \frac{100}{n} \sum_{i=1}^n \left| \frac{D_{\text{cal } i} - D_{\text{mea } i}}{D_{\text{mea } i}} \right| \quad (1)$$

where  $i = \text{ith}$  bridge measurement point;  $D_{\text{cal}}$  = peak of calculated values;  $D_{\text{mea}}$  = peak of measured values; and  $n$  = number of compared pairs of calculated and measured values.

Due to the symmetry of the bridge with respect to the vertical plane passing through the track axis and the planned limitations of the bridge monitoring to the left girder, points on the left side were selected for analyses. Because of the small values of the deflections, Midpoints 7L and 8R were not taken into account. Due to the structural characteristics involving deflections both downward (caused by direct load) and upward (resulting from indirect load—on the other part of the bridge), negative and positive peaks were calculated separately when determining the MAPD.

Following Aloisio et al. (2022), to estimate the degree of similarity between calculated and measured forced vibration time displacement histories (without the part regarding free vibrations), the second parameter, called correlation coefficient (CC), was used. The CC  $\rho(d_{\text{cal}}, d_{\text{mea}})$  was calculated as follows (Stuart and Ord 1995):

$$\rho(d_{\text{cal } i}, d_{\text{mea } i}) = \frac{1}{N-1} \sum_{i=1}^N \left( \frac{d_{\text{cal } i} - \mu_{\text{cal}}}{\sigma_{\text{cal}}} \right) \left( \frac{d_{\text{mea } i} - \mu_{\text{mea}}}{\sigma_{\text{mea}}} \right) \quad (2)$$

where  $i = \text{ith}$  measured or calculated value;  $\mu_{\text{cal}}$  and  $\sigma_{\text{cal}}$  = mean and standard deviation of calculated values;  $\mu_{\text{mea}}$  and  $\sigma_{\text{mea}}$  = mean and standard deviation of measured values, respectively; and  $N$  = number of observations.

The determined parameters (MAPD and CC) for the passage of the test train at speeds from 10 to over 200 km/h (exactly 205 km/h) are shown in Fig. 5. In the case of MAPD,  $n = 2$  (number of compared pairs of calculated and measured values), and in the case of CC,  $N$  varies from 2,030 to 35,250 (number of observations—depending on the cycle duration and sampling rate). Up to the test train speed of about 130 km/h, both MAPD (<5% for MIMM and <7% for MCFM) and CC (>0.99 for MCFM and MIMM) indicate a high agreement between the calculated and measured displacements. From a speed of 180 km/h, the calculated values are no longer as consistent with the measured results. The greatest discrepancies occur at a speed of approximately 205 km/h. In the case of the MIMM, there is also a significant discrepancy at about 180 km/h. Due to smaller deviations of peak values at most speeds of the test train passage and good waveform conformance described by CC, MIMM was adopted for further analysis. The numerical models of the moving load included both concentrated forces and sliding mass over the rails with contact but without the suspension of the train. This may result in different responses for trains at higher speeds.

## Analysis of Bridge Deck Vibrations

A detailed analysis of numerical results for bridge deck vibrations during a train passage with a speed of 205 km/h was conducted. Time histories of accelerations were determined at all points spaced every 0.25 m (acceleration control points) on the beam girder (along the middle line of the bottom and upper surfaces) and concrete slab (along the middle line of the bottom surface). After applying 30-Hz low-pass filtering, for each acceleration control point, extreme values from all waveforms were determined and are marked on the graphs presented in Fig. 6. Comparison of the calculated and measured values was carried out at four points of the girders (dot markers in Fig. 6). Extreme acceleration values occurred at control points of the concrete slab located in the zone between Hanger nos. 3 and 4 and at the end of the slab (looking in the direction of the traveling train). All extreme values were well below the limit value of 3.5 m/s<sup>2</sup>, which is a limit of creating the risk of destabilizing the ballast (Calgaro et al. 2010).

## Results of Monitoring and Numerical Analyses

In addition to data from inclinometers and accelerometers and the displacements determined on their basis, the monitoring system also used external data about train passages: type of train (multiple-unit passenger trains or a separate locomotive with cars), gross weight, and the length of the train. The data were provided by the Railway Traffic Management Centre in an off-line and semiautomatic mode. On the basis of these data from the railway timetable, supplemented with the catalog data of rolling stock manufacturers and determined on the basis of measurements of travel speed, theoretical courses of displacements and acceleration were determined using MIMM at the displacement monitoring point, i.e., at 3–4L. Over the first 8 months of monitoring, on average once a month, the reference sensor (inductive transducer based on the adjacent structure) was installed at the 3–4L point for short comparison tests (Olaszek et al. 2020). Examples of the deflection and bridge deck and hanger acceleration time histories recorded during such tests are shown in Figs. 7 and 8.

The selected examples concern trains with significantly different axle load distributions. Fig. 7 shows the results of bridge behavior during the passage of a locomotive with 14 passenger cars traveling at a speed of about 150 km/h, while Fig. 8 illustrates bridge behavior during the passage of a multiple-unit passenger train moving at a speed of about 200 km/h. The following comparison parameters (presented in the section “Numerical Model Calibration”) for the displacement of forced vibrations were obtained and are presented in Table 3.

The determined parameters comparing the calculated and measured values using the reference method [except for the MAPD<sub>positive</sub> value from Fig. 7(a)] are similar to the analogous parameters determined during dynamic load testing (Fig. 4). The determined parameters comparing the measured values from the inertial method and the reference method confirm the high accuracy of the inertial method for the indirect determination of displacements. This is especially noticeable in the case of negative values where the MAPD is equal to or less than 2.3%.

In a similar way, as shown in Fig. 6, the extreme values from the calculated time histories of vibration accelerations at the control points of the girders and concrete slab were determined and are presented in Figs. 9(a and b). The computations were performed for the train speeds of 150 km/h [responses presented in Fig. 7(b)] and 200 km/h [responses presented in Fig. 8(b)], respectively. In both cases, all extreme values were well below the limit value of 3.5 m/s<sup>2</sup>.

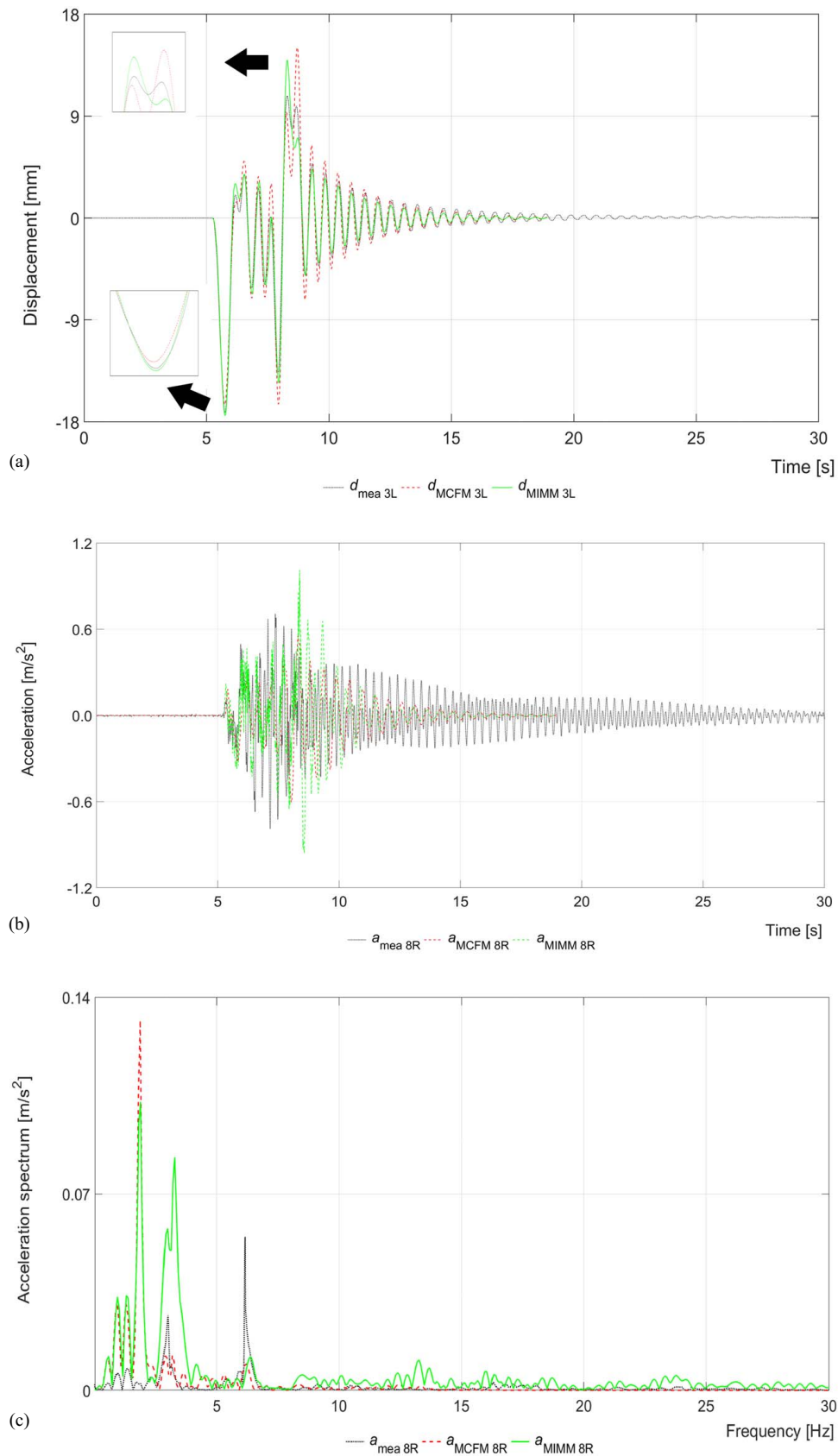


**Fig. 4.** Comparison of measured and calculated (with MCFM and MIMM) values during the passage of a test train at a speed of about 200 km/h: (a) vertical displacement of the beam girder near Hanger no. 3: time history of measured displacement, Line  $d_{\text{mea } 3L}$ ; time history of calculated displacement, Lines  $d_{\text{MCFM } 3L}$  and  $d_{\text{MIMM } 3L}$ ; (b) vertical acceleration of beam girder vibration near Hanger no. 8 (applying the low-pass filter of 30 Hz): time history of measured acceleration, Line  $a_{\text{mea } 8R}$ ; time history of calculated acceleration, Lines  $a_{\text{MCFM } 8R}$  and  $a_{\text{MIMM } 8R}$ ; and (c) acceleration frequency spectra of the measured and calculated bridge deck vibrations.

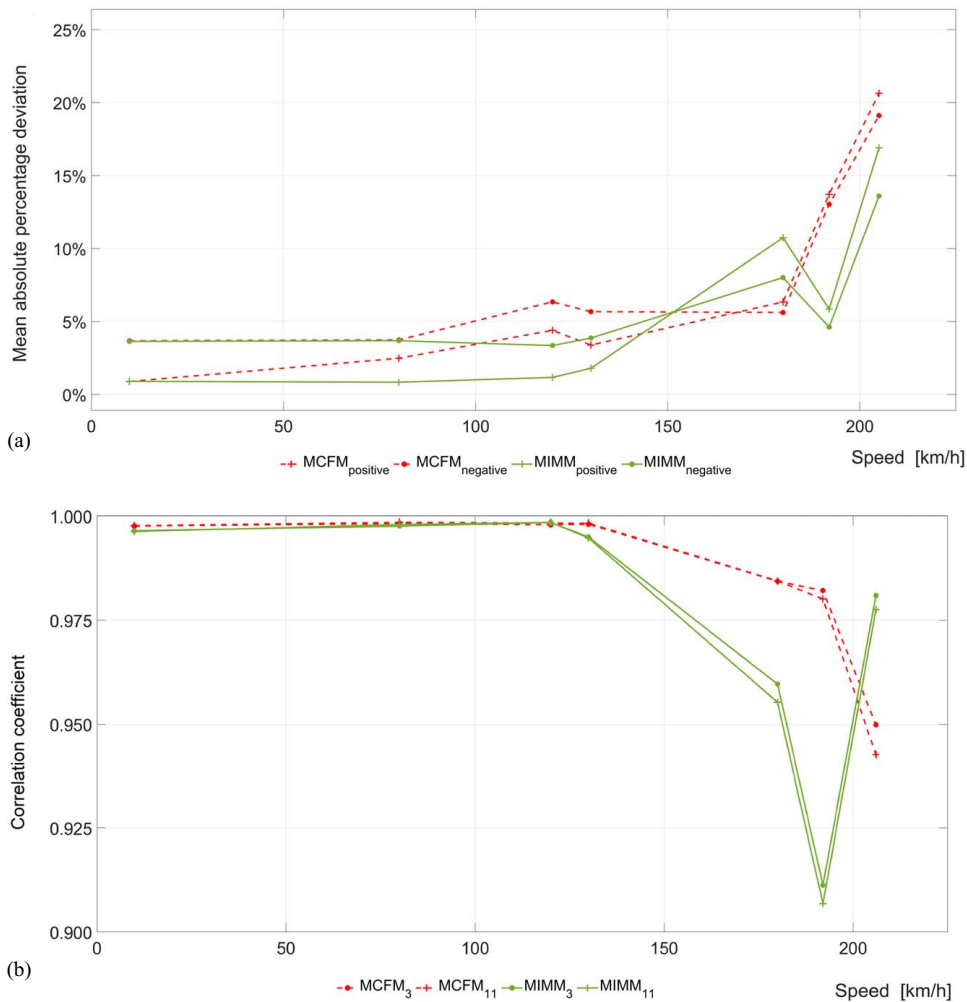


**Fig. 5.** Comparison of the calculated displacements of forced vibrations with those measured: (a) using MAPD calculated as average at Points 3L and 11L separately for negative (dot markers) and positive (plus markers) peaks for both moving load models (MCFM and MIMM); and (b) using CC calculated separately at Points 3L and 11L for both moving load models (MCFM and MIMM).

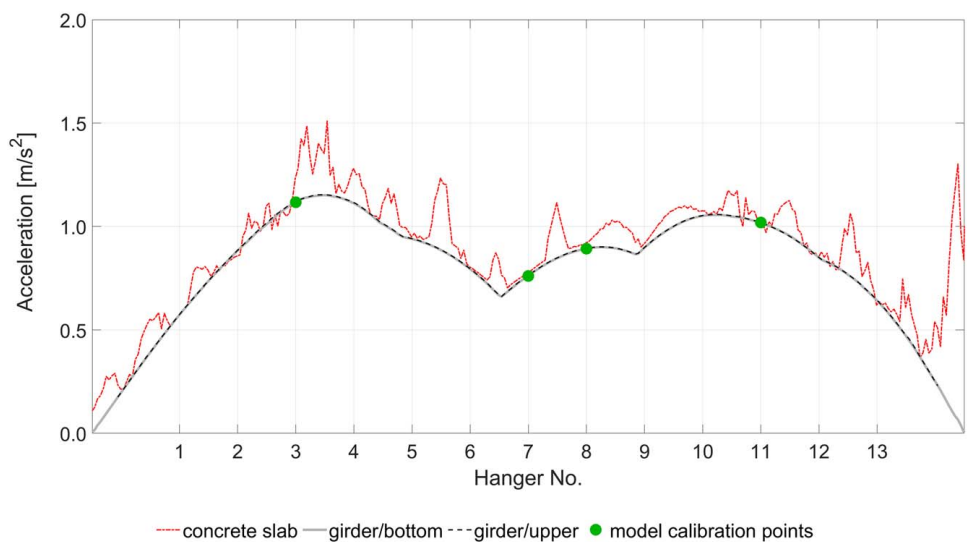


**Fig. 6.** Numerical analysis (MIMM) of acceleration of beam girder (bottom and upper surfaces) and concrete slab vibrations along the span length during the passage of a test train at a speed of about 205 km/h; graphs present the calculated extremal amplitudes of vibration acceleration along the span during train passage; a low-pass filter of 30 Hz was applied. Dots marked points of comparison (during model calibration) of calculated and measured values.

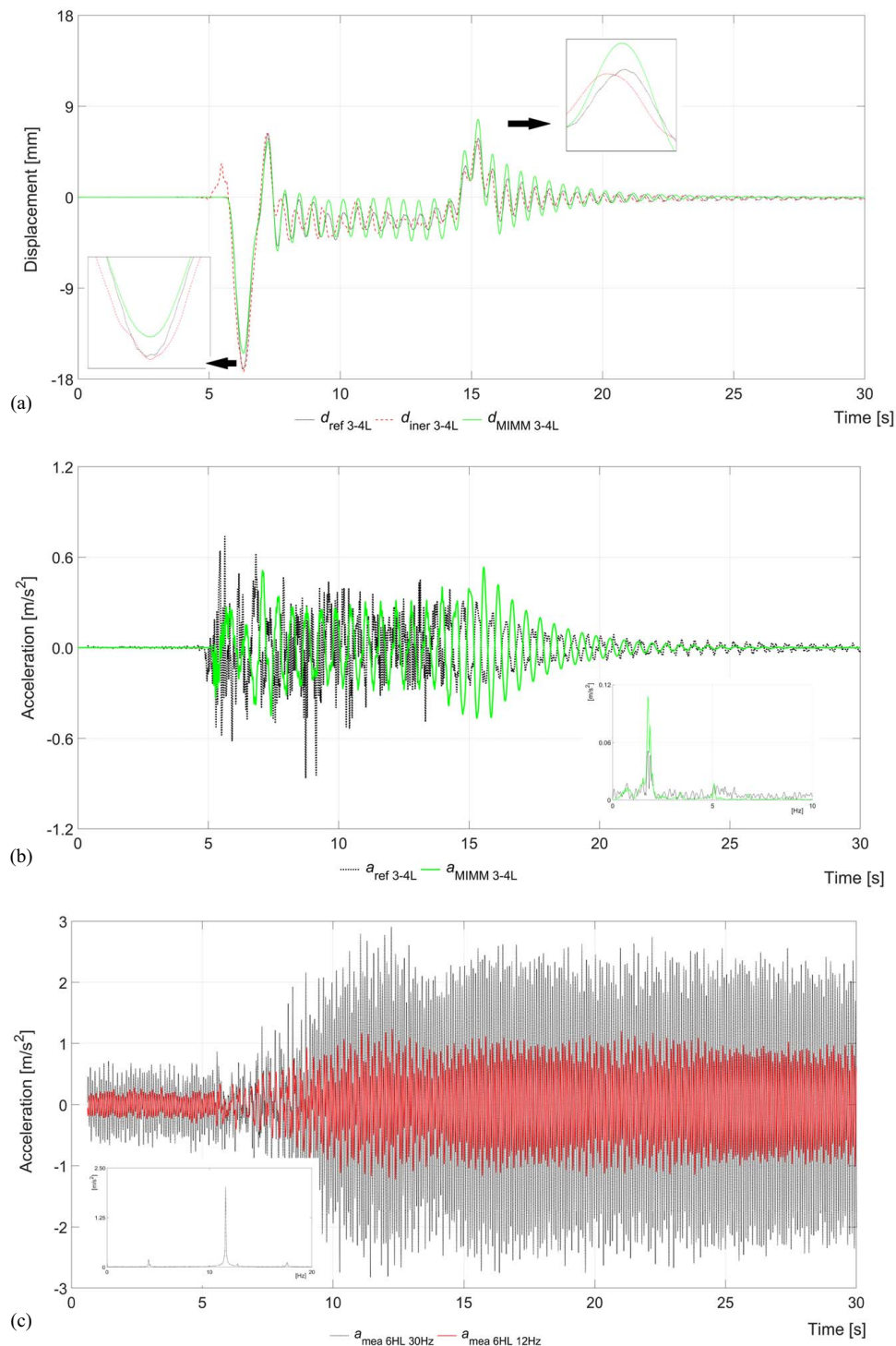


**Fig. 7.** Example of the recorded behavior of the bridge during the passage of a locomotive with 14 passenger cars at a speed of about 150 km/h: (a) time history of the displacement of the beam girder between Hanger nos. 3 and 4—measured with the reference sensor ( $d_{ref\ 3-4L}$ ), measured indirectly using inertial sensors ( $d_{iner\ 3-4L}$ ), and calculated ( $d_{MIMM\ 3-4L}$ ); (b) time history of the acceleration of beam girder vibrations between Hanger nos. 3 and 4—measured with the accelerometer (Line  $a_{mea\ 3-4L}$ ) and calculated (Line  $a_{cal\ MIMM\ 3-4L}$ ) using a low-pass filter of 30 Hz, along with the frequency spectra; (c) time history of the acceleration of Hanger no. 6—measured and low-pass-filtered 30 Hz (Line  $a_{mea\ 6HL\ 30Hz}$ ) and 12 Hz (Line  $a_{mea\ 6HL\ 12Hz}$ ), along with the frequency spectra.

During the train’s passage over the bridge, the extreme deflections occur at 1/4 of the span (usually the highest amplitude when the train enters the bridge—it depends on the train speed) and at 3/4 of the span, when the train leaves the bridge. The displacement amplitude in the middle of the span reaches about 50% of the maximum deflection. This lower value is caused by

the high tensile force in the horizontal girders when the train occupies the entire span. The lower displacement results in a lower acceleration amplitude at specific train speeds.

An analysis of recorded vibrations of the selected hanger was also carried out, and the lowest dominant vibration frequencies were determined. To visualize these vibrations, different low-pass

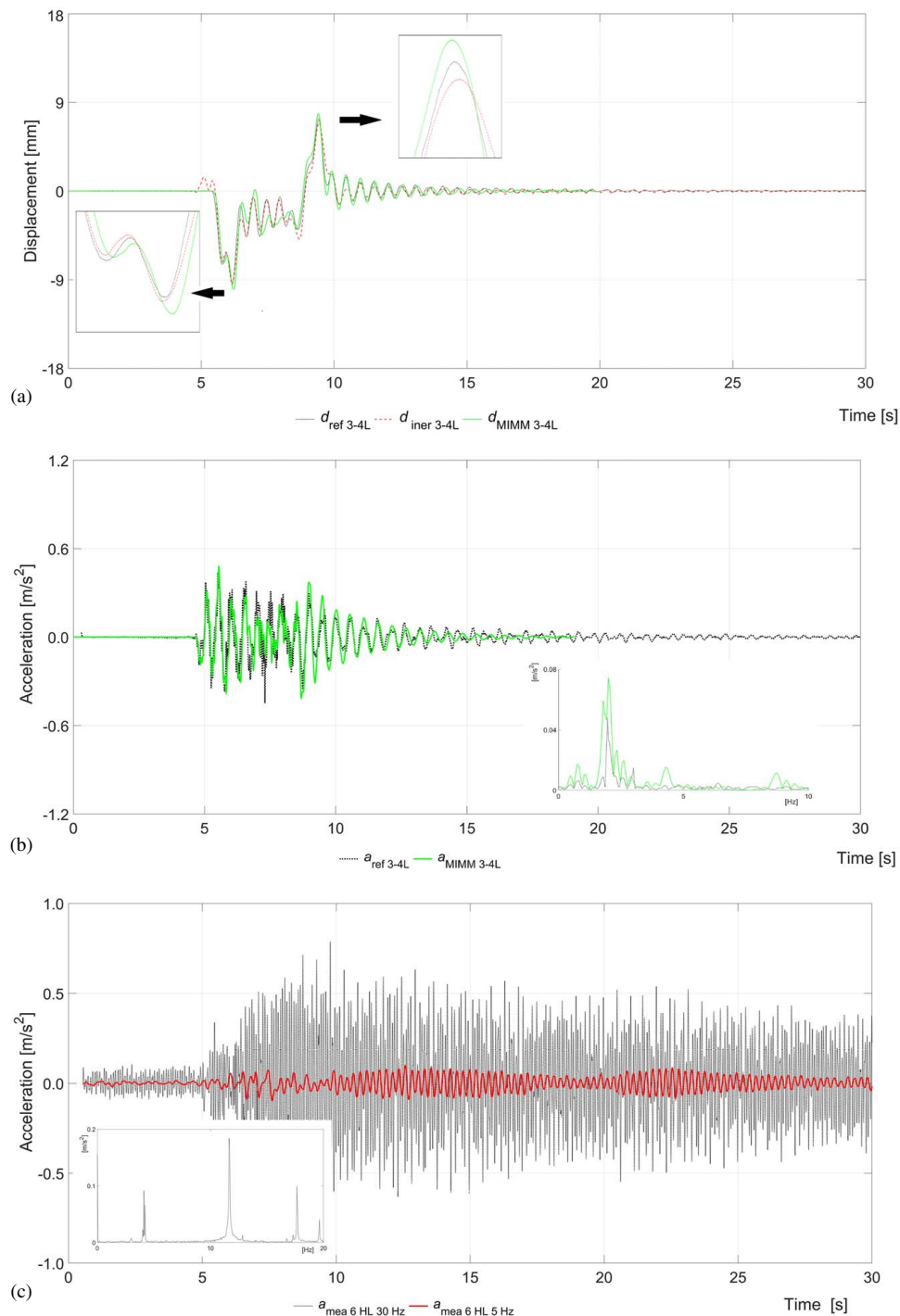


**Fig. 8.** Example of the recorded behavior of the bridge during the passage of a multiple-unit passenger train at a speed of about 200 km/h: (a) time history of the displacement of the beam girder between Hanger nos. 3 and 4—measured with the reference sensor ( $d_{ref\ 3-4L}$ ), measured indirectly using inertial sensors ( $d_{iner\ 3-4L}$ ), and calculated ( $d_{MIMM\ 3-4L}$ ); (b) time history of the acceleration of beam girder vibrations between Hanger nos. 3 and 4—measured with the accelerometer (Line  $a_{mea\ 3-4L}$ ) and calculated (Line  $a_{cal\ MiMM\ 3-4L}$ ) using a low-pass filter of 30 Hz, along with the frequency spectra; and (c) time history of the acceleration of Hanger no. 6—measured and low-pass-filtered 30 Hz (Line  $a_{mea\ 6HL\ 30\ Hz}$ ) and 5 Hz (Line  $a_{mea\ 6HL\ 5\ Hz}$ ), along with the frequency spectra.

filtration thresholds were used in Figs. 7(c) and 8(c) (as illustrated by the frequency spectra). Measurements of vibration accelerations were carried out at 1/4 of the length of the hanger, and on their basis, the extreme values of the displacements occurring at this point were estimated using the double integration method. The vibrations in Fig. 7(c) had a frequency of approximately 11.6 Hz, which corresponded to double amplitudes of vibration

displacement of approximately 0.37 mm, and the vibrations in Fig. 8(c) had a frequency of approximately 4.1 Hz, corresponding to double amplitudes of approximately 0.27 mm. Although these vibrations had much smaller amplitudes compared to the vibrations recorded in the first period of operation—before modifying the hangers by adding masses—there was still weak damping present. In Fig. 8(c), the beating phenomenon resulting from the occurrence

**Table 3.** Comparison of parameters for displacement of forced vibrations during the passage of a locomotive with passenger cars and a multiple-unit passenger train

Train type and speed	MAPD <sub>positive</sub> (%)	MAPD <sub>negative</sub> (%)	$\rho$
Comparison of displacements calculated and measured with the reference method			
Train no. 1, 150 km/h	32.1	9.3	0.945
Train no. 2, 200 km/h	7.2	9.0	0.967
Comparison of displacements measured with inertial sensors and the reference method			
Train no. 1, 150 km/h	5.4	1.4	0.959
Train no. 2, 200 km/h	5.8	2.3	0.971

Notes: Train no. 1 = a locomotive with 14 passenger cars; Train no. 2 = a multiple-unit passenger train.

of two similar vibration frequencies is still visible (4.12 and 4.21 Hz).

During the monitoring of the bridge, significant temperature changes during the 11-month period were recorded: from  $-8^{\circ}\text{C}$  to  $+33^{\circ}\text{C}$  (measurements taken around noon). A significant influence of temperature changes on static structural displacements was observed. Such behavior manifests in long-term and short-term periods for both longitudinal and transversal displacements. For example, the recorded vertical displacement variation at 1/4 span length, measured by the total station, caused by a temperature change of  $28^{\circ}\text{C}$ , reached 10 mm. This topic was discussed in

more detail in Olaszek et al. (2020). A challenge was to model the real structural behavior of the bridge, mainly due to the unknown or difficult to measure temperature distribution over the bridge. However, some simplified temperature change scenarios were considered as follows:

1. A uniform temperature increase of  $5^{\circ}\text{C}$  on the whole structure caused longitudinal displacement up to 4.5 mm at the movable support.
2. A uniform temperature increase of  $5^{\circ}\text{C}$  on the steel structure caused a bending mode of the bridge with displacement in the middle of the span by 3.2 mm.

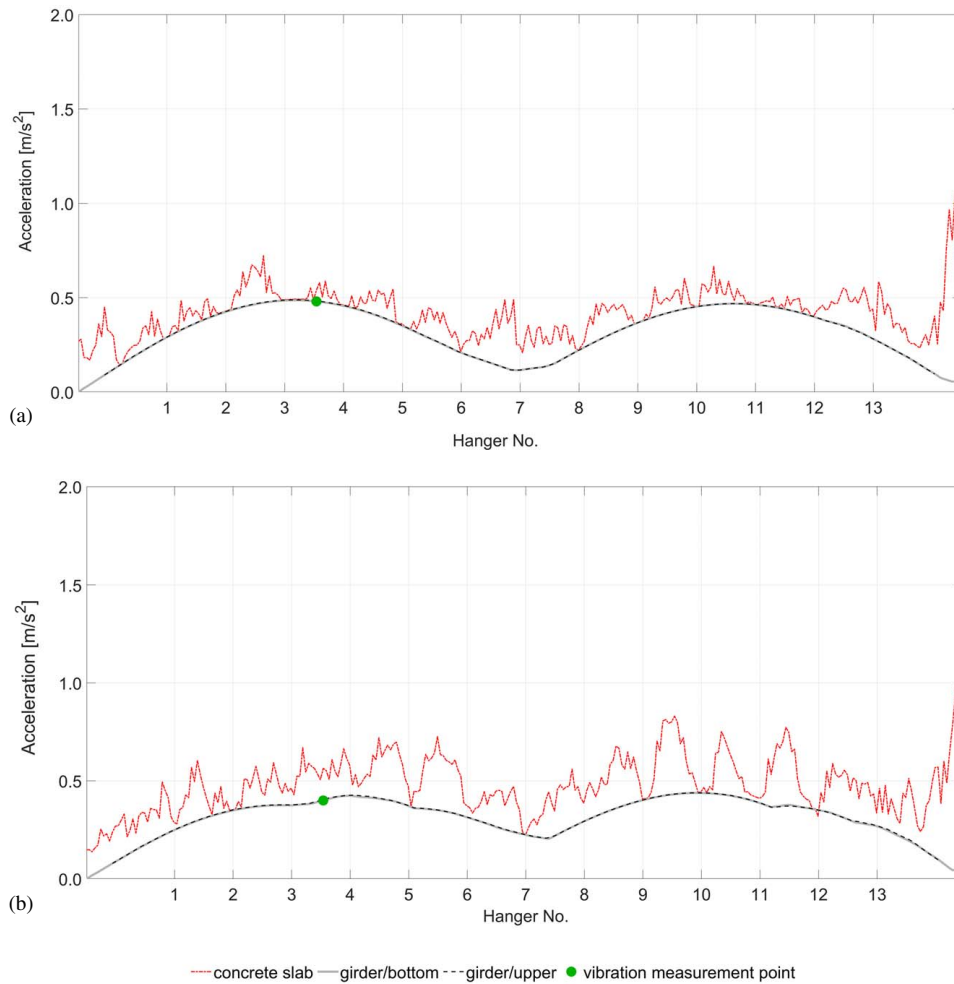


**Fig. 9.** Numerical analysis (MIMM) of the acceleration of beam girder (control points at bottom and upper surfaces) and concrete slab vibrations along the span length during the passage of (a) a locomotive with 14 passenger cars at a speed of about 150 km/h [Fig. 7(b)]; and (b) a multiple-unit passenger train at a speed of about 200 km/h [Fig. 8(b)]. Graphs present the calculated extremal amplitudes of vibration acceleration along the span during the passage of all trains; a low-pass filter of 30 Hz was applied. The dot marked point indicates the vibration measurement at the girder (control points on the upper surface) during monitoring.

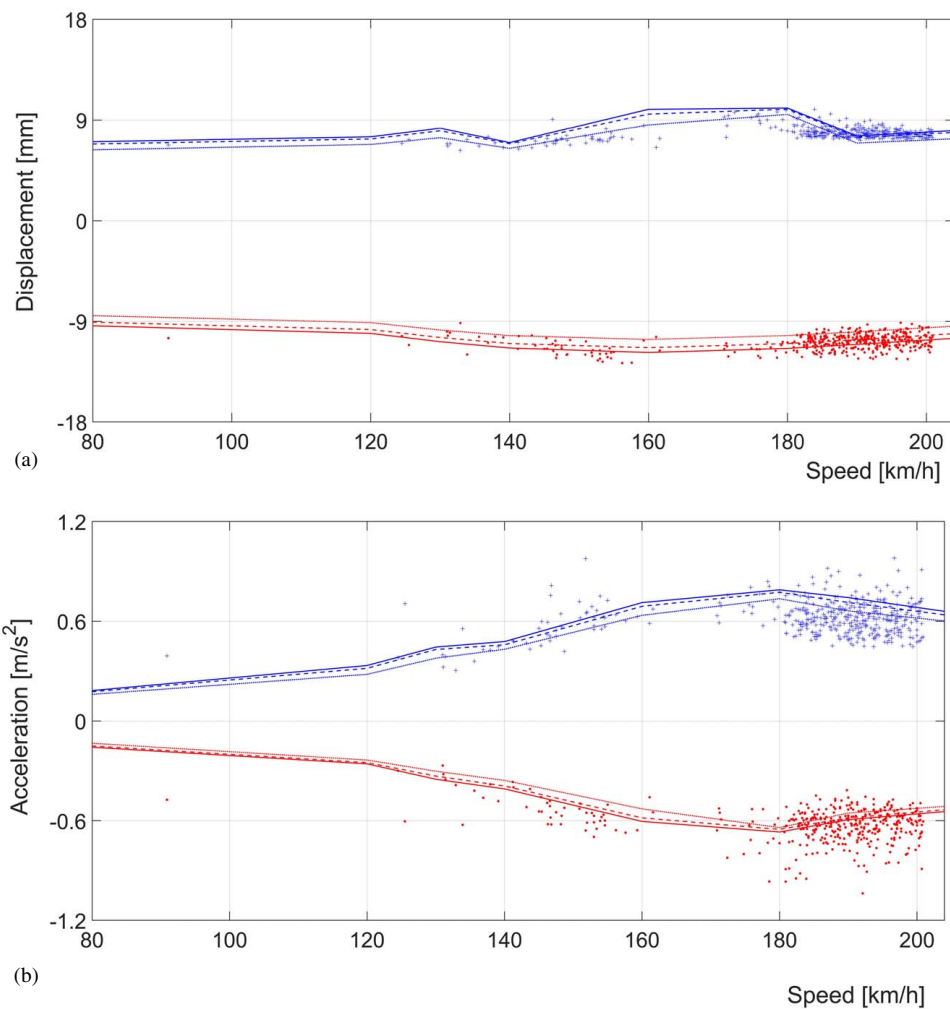


**Fig. 10.** Example of (a) displacement; and (b) acceleration of vibration after 30-Hz low-pass filtering of the beam girder between Hanger nos. 3 and 4 monitoring under a load of multiple-unit passenger trains for 1 month (415 passages): extreme displacement versus speed; upper dot markers, negative; lower plus markers, positive; three upper and lower lines correspond to the numerically determined extreme deflections (MIMM) from an empty train (dotted line), the state of normal use (dashed line), and the fully loaded state foreseen by the manufacturer (solid line).

3. A temperature increase of 5°C on the outer wall of the arch-tied girder caused twisting of the bridge; the heated girder was lifted by 1.5 mm and deflected the other girder by 0.3 mm.

### Summary of Monitoring Results and Discussion

During the monitoring period (11 months), 11,259 trains passed over the viaduct. Cumulative comparative analyses were performed for multiple-unit passenger trains (ED250—popular name Pendolino). It was the only type of train allowed to run at speeds up to 200 km/h during the monitoring period. The monitoring system recorded and correlated 4,692 passages of such trains with the railway timetable. The remaining passenger trains were running at a maximum speed of 160 km/h.

Fig. 10 shows the relationship between the extreme negative and positive displacements and accelerations recorded by the system monitoring versus train speed during the 1-month period—415 passages of the multiple-unit passenger trains ED250. This was the month with a permissible speed of 200 km/h. It should be noted that due to time reserves in the timetable and the proximity of the destination station, not all trains were running at maximum speed. Most of the trains reached the speed of 180–200 km/h.

Fig. 10 illustrates a set of three lines (lower–upper for positive and lower for negative values), each corresponding to the numerically determined extreme deflections [Fig. 10(a)] and accelerations [Fig. 10(b)] from an empty train (dotted lines), the normal state of use (dashed lines), and the fully loaded state foreseen by the manufacturer (solid lines). A comparative analysis of the data from Fig. 10 is presented in Table 4.

Average deviations and average relative deviations of measured displacement and acceleration from the calculated values for the fully loaded state of trains were determined, along with the average speed of train passages. The percentage of train passages with measured displacement and acceleration exceeding the computed ones for the fully loaded state of trains was also reported. In the case of determining displacements, 35% of train passages exceed the values corresponding to the numerically determined fully loaded state of the train, and the average does not exceed 0.5 mm. Fewer than 65% of train passages (with measured values exceeding) exhibit a relative deviation of <5%, while fewer than 95% of passages had a relative deviation of <10%. Taking into account the estimated root-mean-squared deviation of the monitoring system with inertial sensors, which is 0.64 mm (4.8%) for negative extremes and 0.53 mm (8.2%) for positive extremes (Olaszek et al. 2020), it can be concluded that the results of displacement

**Table 4.** Analysis of the 415 passages of the multiple-unit passenger trains (Fig. 10)

Deviations of the measured values from the calculated fully loaded state				Percentage of train passages with measured responses exceeding the computed ones (fully loaded state) with deviation		
Kind of extreme	Average deviation	Average relative deviation (%)	Average measured speed of train passages	Above 0%	Below 5%	Below 10%
				In relation to		
				All train passages (%)	Passages with exceeding (%)	
Vertical displacements						
—	(mm)	—	(km/h)	—	—	—
Negative	0.48	4.4	185	35	62	88
Positive	0.37	4.7	192	27	64	95
Vertical acceleration						
—	(m/s <sup>2</sup> )	—	(km/h)	—	—	—
Negative	0.09	16.3	185	62	22	42
Positive	0.08	13.2	179	15	32	60

Note: Comparison of the measured responses of trains with unknown load status to the calculated responses for the fully loaded state of trains.

measurements and calculations are consistent. The maximum deflection (negative value) of the bridge deck due to the passage of a train is a key parameter determining the correct and safe operation of the structure. In the case of arch structures, an upward displacement of the span is also characteristic. At higher train speeds, the values of these displacements are comparable. Excessive displacements can adversely affect the comfort of train travel and may be associated with excessive accelerations of the bridge structure, which can detrimentally impact the stability of the railway ballast. Therefore, it can be concluded that the bridge did not show excessive displacements caused by multiple-unit passenger trains ED250 passing at different speeds. In the case of vibration acceleration measurements, there were much greater discrepancies between measurements and calculations; 62% of train passages exceeded the values corresponding to the numerically determined fully loaded state, but the average value was low and did not exceed 0.1 m/s<sup>2</sup>. Fewer than 22% of train passages (with measured values exceeding) showed a relative deviation of <5%, while fewer than 42% of crossings exhibited a relative deviation of <10%. The highest recorded vibration acceleration was equal to 1.04 m/s<sup>2</sup>.

Taking into account the proportions in Fig. 9(b), the extreme acceleration on the concrete slab can be numerically estimated at 3.35 m/s<sup>2</sup>, which is below the limit value of 3.5 m/s<sup>2</sup>. Only the point marked with a dot is related to the measurement data. In fact, the accelerometer was installed on the girder (steel structure) and compared with the extreme accelerations computed for the steel girder and the concrete slab [shown in Fig. 9(b) as interpolation lines]. The accelerations were obtained for uniformly distributed points on the girder (along the centerline of the upper and bottom surfaces) and the concrete slab (along the centerline of the bottom surface).

In addition, it should be noted that the analytically determined extreme amplitudes of accelerations are not repetitive cyclical vibrations but only of a single impulse occurring when the train leaves the bridge span. According to Zacher and Baeßler (2008), such (impulse) vibrations are not dangerous for the stability of the railway ballast.

While monitoring, it was determined that hanger vibrations had no notable influence on the monitored displacements and accelerations of bridge deck vibrations when trains passed at high speeds. Supplementary numerical analyses were also conducted to assess the influence of hanger tension and temperature changes on the bridge vibrations. Modal analysis revealed that changes in the

design hanger tension force had a negligible impact on natural frequencies and mode shapes. By uniformly reducing the tension force in all hangers to up to 1/3 of their designed values, a numerical analysis showed no significant perturbation in the dynamic behavior of the structure; however, it did influence the vibrations of the hangers themselves (local modes). This is due to significant stiffness differences between the main girders and the hangers. A similar result was obtained for uniform temperature changes across the structure. However, in the case of nonuniform temperature variations (e.g., an increase in the temperature of steel elements while maintaining the temperature of the concrete slab or an increase in the temperature of sun-exposed structural elements), the numerical calculations demonstrated the susceptibility of the bridge to deformations that could lead to changes in hanger tension and consequently may cause resonance phenomenon of different hangers for different external conditions.

## Conclusions

This paper presents the results of a year-long monitoring of a steel arch-suspended railway bridge. Structures of this type allow for significant span lengths and are cost-effective to build, but due to potential corrosion, they also require regular maintenance. The implemented monitoring system recorded signals from installed inertial sensors (inclinometers and accelerometers), which were used to analyze the vibrations of the structure (e.g., excessive hanger vibrations), including the assessment of structural deflections indirectly. Vibration analysis was supported by a numerical model of the bridge, calibrated using test train passages with known axle loads and speeds. Two variants of moving loads were considered for numerical calculations: noninertial (modeled by a moving system of concentrated forces) and inertial (modeled by a moving system of masses sliding on the rails). It should be emphasized that the numerical analysis of vibrations induced by high-speed train passages is a complex task and should be supported by experimental studies.

From the conducted research, the following conclusions can be drawn:

1. The monitoring results demonstrate that monitoring the bridge's displacements using an indirect method, utilizing data from a limited number of inclinometers and accelerometers, is feasible. The obtained time-dependent displacements are consistent with

- numerical results and measurements. The conducted research also positively verified the possibility of bridge deck vibrations.
- The developed numerical model, calibrated using both quasi-static and high-speed testing train passages, provides additional information about the overall structural vibrations, facilitating the interpretation of outcomes of the monitoring system.
  - In the case of this specific structure, the monitoring system provides near real-time information about excessive bridge deck and hanger vibrations. The measurement data were transmitted to the data center after each train passage.
  - The monitoring system allows for long-term analysis of measurement data and provides the means for early detection of potential excessive vibrations or deflections in the structure that could lead to premature failure.
  - During the monitoring, no significant impact of immoderate hanger vibrations on the monitored displacements and accelerations of the bridge deck during the passage of trains at speeds up to 200 km/h was found.

All engineering structures, especially arch-type structures, require meticulous construction, and in the case of hanger installations, there should always be provisions for adjusting their tension, allowing for the correction of construction imperfections in the girders and arch, as well as inaccuracies in tension arising during hanger installation through welding them to the bridge deck.

## Data Availability Statement

The collected data, together with the train timetable and the detailed design geometry of the bridge, have been made confidential by PKP Polskie Linie Kolejowe S.A. (Polish Railways); however, upon request, the skeleton batch files for computing dynamic responses used in Abaqus software can be made available.

## Acknowledgments

The authors thank the members of the team who completed the presented part of the project, including Robert Czachowski, Małgorzata Mazanek, Marek Łaqoda, Tomasz Wierzbicki, Paweł Nurek, and Ewa Twardosz from the Road and Bridge Research Institute; Kazimierz Szadkowski; and Directors, Main Engineers, and Bridge Diagnosticians from the Railway Track Development and Construction Unit of PKP Polskie Koleje Państwowe S.A. Special thanks go to Krzysztof Żółtowski from Gdańsk University of Technology for consultations during the analysis of the monitoring results. Part of the hanger vibration research was carried out in cooperation with Gdańsk University of Technology and the Aspekt company. Part of the project was carried out within the framework of Applied Research Projects, financed by the National Centre for Research and Development, Poland, from 2015 to 2018 (Grant agreement PBS3/B9/36/2015). The authors also acknowledge the support of the National Science Centre, Poland (Grant agreement 2018/31/B/ST8/03152).

## References

- Abaqus. 2024. *SIMULIA user assistance*. Vélizy-Villacoublay, France: Dassault Systèmes SE.
- Aloisio, A., M. M. Rosso, and R. Alaggio. 2022. "Experimental and analytical investigation into the effect of ballasted track on the dynamic response of railway bridges under moving loads." *J. Bridge Eng.* 27 (10): 04022085. [https://doi.org/10.1061/\(ASCE\)BE.1943-5592.0001934](https://doi.org/10.1061/(ASCE)BE.1943-5592.0001934).
- Andersson, A., A. O'Connor, and R. Karoumi. 2015. "Passive and adaptive damping systems for vibration mitigation and increased fatigue service life of a tied arch railway bridge." *Comput.-Aided Civ. Infrastruct. Eng.* 30 (9): 748–757. <https://doi.org/10.1111/mice.12116>.
- Berthelley, J. 2018. "Evaluation regarding fatigue for various type of hangers used for tied arch bridges." *Procedia Eng.* 213: 426–436. <https://doi.org/10.1016/j.proeng.2018.02.042>.
- Bleja, M., and K. Żółtowski. 2021. "FEM dynamic analysis of the hangers in a steel arch railway viaduct." *Buider* 292 (11): 44–49. <https://doi.org/10.5604/01.3001.0015.4166>.
- Calçada, R., A. Cunha, and R. Delgado. 2002. "Dynamic analysis of metallic arch railway bridge." *J. Bridge Eng.* 7 (4): 214–222. [https://doi.org/10.1061/\(ASCE\)1084-0702\(2002\)7:4\(214\)](https://doi.org/10.1061/(ASCE)1084-0702(2002)7:4(214)).
- Calgaro, J.-A., M. Tschumi, and H. Gulvanessian. 2010. *Designers' guide to Eurocode 1: Actions on bridges: EN 1991-2, EN 1991-1-1, -1-3 to -1-7 and EN 1990 Annex A2*. London: Thomas Telford.
- Ding, Y., Y. An, and C. Wang. 2016. "Field monitoring of the train-induced hanger vibration in a high-speed railway steel arch bridge." *Smart Struct. Syst.* 17 (6): 1107–1127. <https://doi.org/10.12989/SSS.2016.17.6.1107>.
- Ding, Y.-L., H.-W. Zhao, L. Deng, A.-Q. Li, and M.-Y. Wang. 2017. "Early warning of abnormal train-induced vibrations for a steel-truss arch railway bridge: Case study." *J. Bridge Eng.* 22 (11): 05017011. [https://doi.org/10.1061/\(ASCE\)BE.1943-5592.0001143](https://doi.org/10.1061/(ASCE)BE.1943-5592.0001143).
- Duan, Y. F., S. K. Wu, S. M. Wang, J. D. Yau, Y. Q. Ni, and C. B. Yun. 2022. "Train-induced dynamic behavior and fatigue analysis of cable hangers for a tied-arch bridge based on vector form intrinsic finite element." *Int. J. Struct. Stab. Dyn.* 22 (12): 2250136. <https://doi.org/10.1142/S021945542250136X>.
- Fricke, W. 2003. "Fatigue analysis of welded joints: State of development." *Mar. Struct.* 16 (3): 185–200. [https://doi.org/10.1016/S0951-8339\(02\)00075-8](https://doi.org/10.1016/S0951-8339(02)00075-8).
- Ju, S.-H., and H.-T. Lin. 2003. "Numerical investigation of a steel arch bridge and interaction with high-speed trains." *Eng. Struct.* 25 (2): 241–250. [https://doi.org/10.1016/S0141-0296\(02\)00148-7](https://doi.org/10.1016/S0141-0296(02)00148-7).
- Klinger, C., T. Michael, and D. Bettge. 2014. "Fatigue cracks in railway bridge hangers due to wind induced vibrations—Failure analysis, measures and remaining service life estimation." *Eng. Fail. Anal.* 43: 232–252. <https://doi.org/10.1016/j.engfailanal.2014.02.019>.
- Lacarbonara, W., and V. Colone. 2007. "Dynamic response of arch bridges traversed by high-speed trains." *J. Sound Vib.* 304 (1–2): 72–90. <https://doi.org/10.1016/j.jsv.2007.01.037>.
- Link, M., M. Weiland, and F. Yu. 2002. "Modal analysis of railway bridge hangers using artificial and ambient excitation." *J. Phys. IV* 12 (11): 101–110. <https://doi.org/10.1051/jp4:20020481>.
- Malm, R., and A. Andersson. 2006. "Field testing and simulation of dynamic properties of a tied arch railway bridge." *Eng. Struct.* 28 (1): 143–152. <https://doi.org/10.1016/j.engstruct.2005.07.011>.
- Nakutis, Ž., and P. Kaškonas. 2011. "Bridge vibration logarithmic decrement estimation at the presence of amplitude beat." *Measurement* 44 (2): 487–492. <https://doi.org/10.1016/j.measurement.2010.11.012>.
- Olaszek, P., I. Wyczałek, D. Sala, M. Kokot, and A. Świercz. 2020. "Monitoring of the static and dynamic displacements of railway bridges with the use of inertial sensors." *Sensors* 20 (10): 2767. <https://doi.org/10.3390/s20102767>.
- Rao, J. S. 2017. *Simulation based engineering in solid mechanics*. Cham, Switzerland: Springer.
- Ribeiro, D., R. Calçada, R. Delgado, M. Brehm, and V. Zabel. 2012. "Finite element model updating of a bowstring-arch railway bridge based on experimental modal parameters." *Eng. Struct.* 40: 413–435. <https://doi.org/10.1016/j.engstruct.2012.03.013>.
- Salamak, M., D. C. Nguyen, A. Katunin, and G. Poprawa. 2023. "Finite element model updating of steel bridge structure using vibration-based structural health monitoring system: A case study of railway steel arch bridge in Poland." In *Experimental vibration analysis for civil engineering structures*, edited by M. P. Limongelli, P. F. Giordano, S. Quqa, C. Gentile, and A. Cigada, 371–380. Lecture Notes in Civil Engineering. Cham, Switzerland: Springer.

- Stuart, A., and J. K. Ord. 1995. *Kendall's advanced theory of statistics: Classical inference and relationship*. 5th ed. London: Griffin.
- Zacher, M., and M. Baeßler. 2008. "Dynamic behaviour of ballast on railway bridges." In *Dynamics of high-speed railway bridges*, edited by R. Delgado, R. Calcada, J. M. Goicolea, and F. Gabaldon, 109–122. Boca Raton, FL: CRC Press.
- Zeng, Q., C. D. Stoura, and E. G. Dimitrakopoulos. 2018. "A localized Lagrange multipliers approach for the problem of vehicle-bridge-interaction." *Eng. Struct.* 168: 82–92. <https://doi.org/10.1016/j.engstruct.2018.04.040>.
- Zhao, H.-W., Y.-L. Ding, S. Nagarajaiah, and A.-Q. Li. 2019. "Behavior analysis and early warning of girder deflections of a steel-truss arch railway bridge under the effects of temperature and trains: Case study." *J. Bridge Eng.* 24 (1): 05018013. [https://doi.org/10.1061/\(ASCE\)BE.1943-5592.0001327](https://doi.org/10.1061/(ASCE)BE.1943-5592.0001327).
- Zhong, W., Y.-l. Ding, Y.-s. Song, and H.-w. Zhao. 2018. "Fatigue behavior evaluation of full-field hangers in a rigid tied arch high-speed railway bridge: Case study." *J. Bridge Eng.* 23 (5): 05018003. [https://doi.org/10.1061/\(ASCE\)BE.1943-5592.0001235](https://doi.org/10.1061/(ASCE)BE.1943-5592.0001235).